CMLS, Cell. Mol. Life Sci. 60 (2003) 2356–2370
1420-682X/03/112356-15
DOI 10.1007/s00018-003-3072-1

CMLS Cellular and Molecular Life Sciences

Review

Structure and morphogenesis of bacteriophage T4

P. G. Leiman [a,*], S. Kanamaru [a], V. V. Mesyanzhinov [b], F. Arisaka [c] and M. G. Rossmann [a]

[a] Department of Biological Sciences, Purdue University, 915 W. State Street, West Lafayette, Indiana 47907-2054 (USA), Fax +1 765 496 1189, e-mail: leiman@purdue.edu
[b] Laboratory of Molecular Bioengineering, Shemyakin-Ovchinnikov Institute of Bioorganic Chemistry, 16/10 Miklukho-Maklaya Street, 117997 Moscow (Russia)
[c] Department of Life Science, Faculty of Bioscience and Biotechnology, Tokyo Institute of Technology, 4259 Nagatsuta, Midori-ku, Yokohama 226-8501 (Japan)

Received 18 February 2003; received after revision 16 April 2003; accepted 9 May 2003

Abstract. Bacteriophage T4 is one of the most complex viruses. More than 40 different proteins form the mature virion, which consists of a protein shell encapsidating a 172-kbp double-stranded genomic DNA, a 'tail,' and fibers, attached to the distal end of the tail. The fibers and the tail carry the host cell recognition sensors and are required for attachment of the phage to the cell surface. The tail also serves as a channel for delivery of the phage DNA from the head into the host cell cytoplasm. The tail is attached to the unique 'portal' vertex of the head through which the phage DNA is packaged during head assembly. Similar to other phages, and also herpes viruses, the unique vertex is occupied by a dodecameric portal protein, which is involved in DNA packaging.

Key words. Bacteriophage T4; baseplate; contractile tail; DNA packaging; fibrous protein; phage infection; prolate head capsid.

Introduction

Viruses are ubiquitous and obligatory parasites of animals, plants, and bacteria. Although all viruses require a living host for reproduction, host range diversity is a consequence of differences in virus structure and function. A virus consists of a genome encapsidated into a protein or proteolipid shell. The shell protects the genome when the virus is transmitted between hosts. In addition, the shell carries the host recognition sensors and, once a susceptible host has been located, delivers the viral genome into the host.

Bacterial viruses, or bacteriophages, range markedly in their complexity from simple spherical viruses, whose genome size is only about 5 kbp (e.g., bacteriophage ϕX174) [1], to complex viruses with genomes of more than 280 kbp (e.g. bacteriophage ϕKZ) [2]. Several families of bacteriophage have a special tube-like organelle called a 'tail,' absent in other bacterial, animal, and plant viral families, attached to one of the vertices of the shell. The tail is used during infection for penetration through the cell envelope and subsequent DNA translocation from the shell into the host cell. The host cell receptor recognition molecules are attached to the tail, which helps to coordinate the processes of host recognition and DNA delivery.

Bacteriophage T4 is a double-stranded DNA (dsDNA) tailed virus that infects *Escherichia coli* (fig. 1). It is one of the most complex viruses, with a genome that contains 274 open reading frames out of which more than 40 encode structural proteins [3]. The mature virus, or 'virion,' consists of a 1150 Å-long, 850 Å-wide prolate head with hemicosahedral ends [4] encapsidating the genomic DNA; a 1000 Å-long, 210 Å-diameter cocylindrical contractile tail [5], terminated with a 460 Å-diameter baseplate [6]; and six

* Corresponding author.

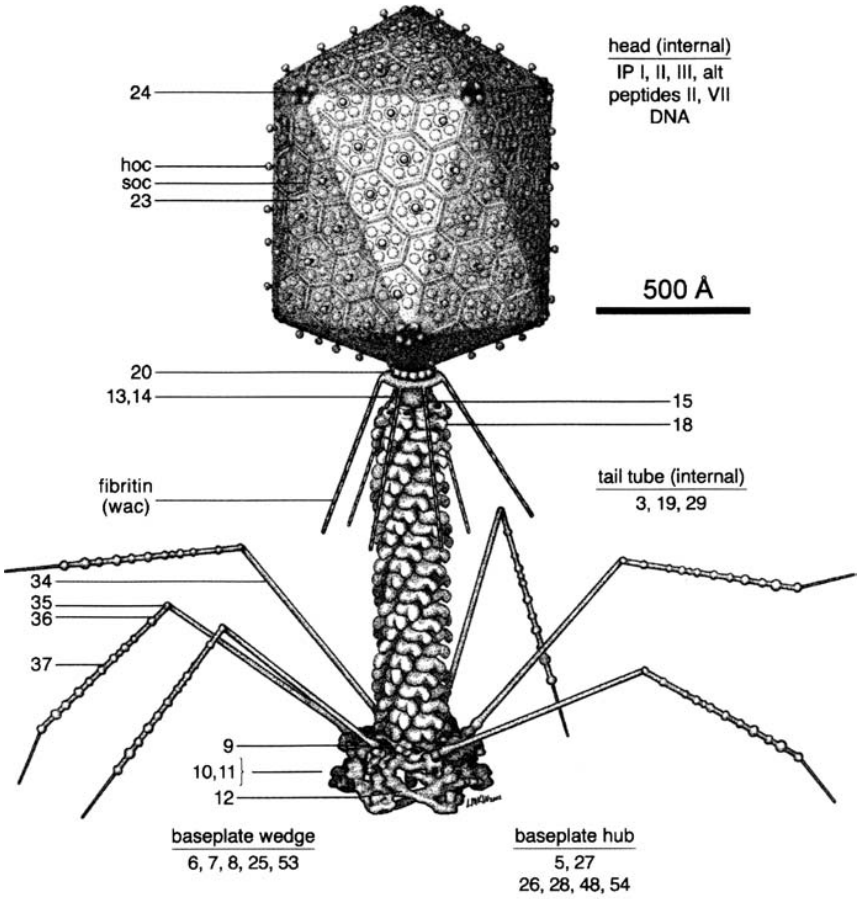

Figure 1. Structure of bacteriophage T4 (modified from Eiserling & Black [16]). The proteins comprising the virion are labeled with their corresponding gene number or name. [Provided by Fred Eiserling, University of California, Los Angeles.]

1450 Å-long fibers attached to the baseplate [7]. The head, tail, and fibers assemble via independent ordered pathways and join together to form a mature virus particle.

Unlike animal viruses, infection of host cells by tailed bacteriophages is highly efficient – only one bacteriophage T4 particle is required, in general, to infect a host cell [8]. Upon infection, the phage shuts down host-specific nucleic acid and protein syntheses, thus ensuring production of only its own components in amounts sufficient to assemble up to 200 progeny virus particles per infected cell. The efficiency of the infection process and the large genome of bacteriophage T4, in which only half of the genes are necessary for proliferation on *E. coli*, contribute to the diversity of the phages from the T4-like family, a subgroup of *Myoviridae* [9]. These phages propagate on a wide range of bacterial hosts that grow in diverse environments [9–12].

The structures of the bacteriophage T4 head, tail, and fibers have been studied using various techniques [for reviews see refs 13–15]. When combined with extensive biological, genetic, and biochemical data, such as the results from complementation assay studies and cross-linking analysis, these studies provide a structural model of bacteriophage T4 [16]. Recent advances in electron microscopy, X-ray crystallography, and computing power have extended the structural knowledge of T4 to higher resolution. This review focuses on these advances.

Bacteriophage T4 head

Head structure

The head of bacteriophage T4 is composed of more than 3000 polypeptide chains of at least 12 kinds of protein (table 1) and a 172-kbp dsDNA chromosome, which comprises 102% of the unique region of about 169 kbp. The molecular weight (MW) of the head and the genomic DNA are 194 MDa and 112 MDa, respectively [17]. The shell has icosahedral ends and a cylindrical equatorial midsection [4, 18] with a unique portal vertex where the phage tail is attached. The icosahedral caps ($T = 13$ laevo [19]) and the midsection ($Q = 21$ [4]) are formed by 160

Table 1. Protein compositions of the T4 prohead and mature head (modified from Black et al. [13]).

Gene	Prohead		Head		Location
	mass (kDa)	copy number	mass (kDa)	copy number	
23	56.0	960	48.7	960	shell, major capsid protein
20	61.0	12	61.0	12	shell, portal vertex
24	48.4	55	46.0	55	shell, fivefold vertices
soc	–	0	9.7	840	shell, outer surface
hoc	–	0	39.1	160	shell, outer surface
22	29.8	576	2.5	115	internal (scaffold)
21	23.2	72	18.5	3	internal (scaffold)
IPIII	21.7	370	20.4	370	internal (scaffold)
IPI	10.0	360	8.5	360	internal (scaffold)
IPII	11.1	360	9.9	360	internal (scaffold)
alt	76.8	40	75.9	40	internal (portal vertex)
68	17.0	240	–	0	internal
67	9.1	341	3.9	134	internal

Copy numbers of the shell proteins are derived from the EM studies [17, 20, 25]. Copy numbers of the internal proteins are based on the SDS-PAGE analysis of Onorato et al. [95] and Isobe et al. [96].

hexamers of gene product (gp)23*[1]. The 12 pentagonal vertices of the icosahedron are occupied by 11 pentamers of gp24* [20] and one dodecamer of gp20 [21], which substitutes the 12 pentamer of gp24* at the portal vertex. The shell is decorated on the outside with gp hoc and gp soc (highly antigenic outer capsid protein and small outer capsid protein, respectively) [4, 22]. The latter two proteins are non-essential for phage morphogenesis, although biochemical data indicate that at least gp soc helps to maintain head integrity in extreme environmental conditions [23, 24].

A number of mutations in the capsid proteins (reviewed in Black et al. [13]) lead to formation of heads with different *Q* numbers [18]: isometrics ($Q = T = 13$), petites or intermediates ($Q = 17$), wild type (Q = 21), and giants ($Q > 21$). The semi-spherical ends in these mutants have the same width as the $T = 13$ caps, but the lengths of their midsection are different. The isometric heads are icosahedral whereas the petites, the wild type, and the giants are prolate. The isometric variants of heads have been studied by cryo-electron microscopy (cryoEM). Three-dimensional (3D) maps of the empty capsids with and without gp soc [25] and of DNA-filled capsids [20] have been determined at 27-Å resolution and at 15-Å resolution, respectively. The head diameter was found to vary from ~973 Å along the fivefold axes to ~879 Å along the threefold and twofold axes (fig. 2). As expected for a $T = 13$ particle, the head is composed of 120 hexamers of gp23* and 11 pentamers of gp24*. They form a shell that is about 30 Å thick, encapsidating the genomic DNA (fig. 3). Gp soc is a rod-like molecule (~39 × 27 × 14 Å),

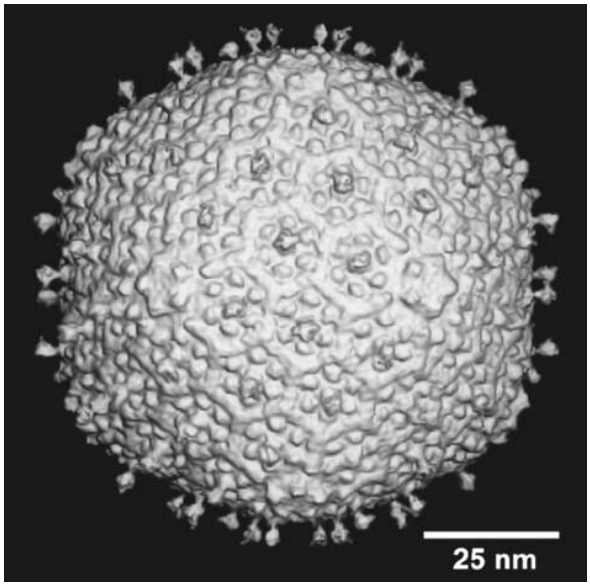

Figure 2. Shaded-surface representation of the 3D cryoEM reconstruction of the T4 isometric heads. The view is along a twofold axis of the icosahedron. The prominent balloon-shaped projections are gp hoc molecules. A total of 120 such molecules extend outward from the center of each gp23* hexamer in the capsid. (Reprinted with permission from Olson et al. [20]. Copyright 2001, Academic Press.)

which forms a continuous mesh on the surface of gp23* hexamers (figs 2, 4). Every gp soc molecule binds between two gp23* subunits, but not between gp23* and gp24* (fig. 4) and, therefore, gp soc does not bind around the gp24* pentamers. Gp soc forms trimers at the meeting points of three gp23* hexamers, although when purified from the phage or when expressed in *E. coli*, it is a monomer in solution [25]. Since gp soc has been shown to stabilize the head structure in extreme environmental conditions, it might promote capsid stabilization by com-

[1] According to phage genetics usage, gpX* signifies the product of maturation produced by the cleavage of gpX to gpX*. An explanation of *T* and *Q* numbers that describe prolate head symmetry is reviewed in reference 18.

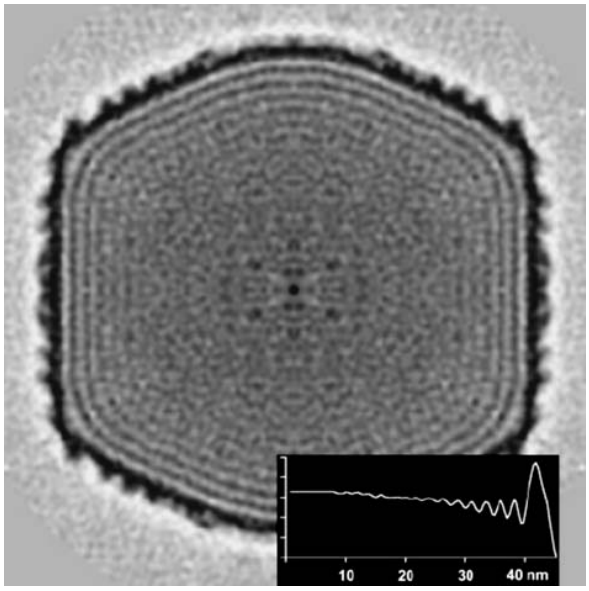

Figure 3. Central section of the reconstructed T4 head density map viewed along a twofold axis. The DNA and protein density are dark. The concentric dark layers beneath the outer capsid shell are attributed to the densely packaged dsDNA. The inset plots the spherically averaged density, computed from the 3D reconstruction, as a function of radius. The highest-density peak at the far right of the plot corresponds to the protein density in the outer capsid shell (~3.0 nm thick). Eight progressively smaller peaks between radii of 38 and 22 nm arise from the condensed layers of dsDNA. The spacing between successive rings is ~2.4 nm, which closely agrees with previous measurements of close-packed DNA in bacteriophage T7 [56]. (Reprinted with permission from Olson et al. [20]. Copyright 2001, Academic Press.)

pensating for unfavorable interactions left on the gp23* surface upon prohead maturation [23, 24]. Gp hoc is a balloon-shaped molecule and extends to ~50 Å away from the shell surface (figs 2, 4). Its protruding part is composed of two domains: a rounded base (~19 Å high) and a globular head (~20 Å wide, 24 Å high) connected by a thin neck region. The overall mass of the protrusion is about 12 kDa, suggesting that up to two-thirds of gp hoc might be inserted in the center of each gp23* hexamer. The function of gp hoc is unknown.

The gp20 dodecamer, which occupies one of the 12 five-fold vertices, could not be detected in the cryoEM maps reported by either Iwasaki et al. [25] or Olson et al. [20] due to the 532-icosahedral symmetry imposed by the reconstruction, causing the gp20 density to be equivalenced with the 11 pentamers of gp24*. The density in the vicinity of gp24* pentamers had about the same magnitude as the rest of the gp23* shell, suggesting that the distortion of the shell, introduced by the gp20 dodecamer around the unique portal vertex, is minimal.

Head morphogenesis

Assembly of the T4 head (fig. 5) starts with the formation of the gp20–gp40 membrane-spanning initiation complex at the inner side of the cytoplasmic membrane [26]. The function of gp40 is unclear, since it is not present in the assembled heads, but it renders gp20 competent to start the assembly process [27]. Subsequently, gp21, gp22, gp67, gp68, IPI, IPII, IPIII, and gp alt (table 1) at-

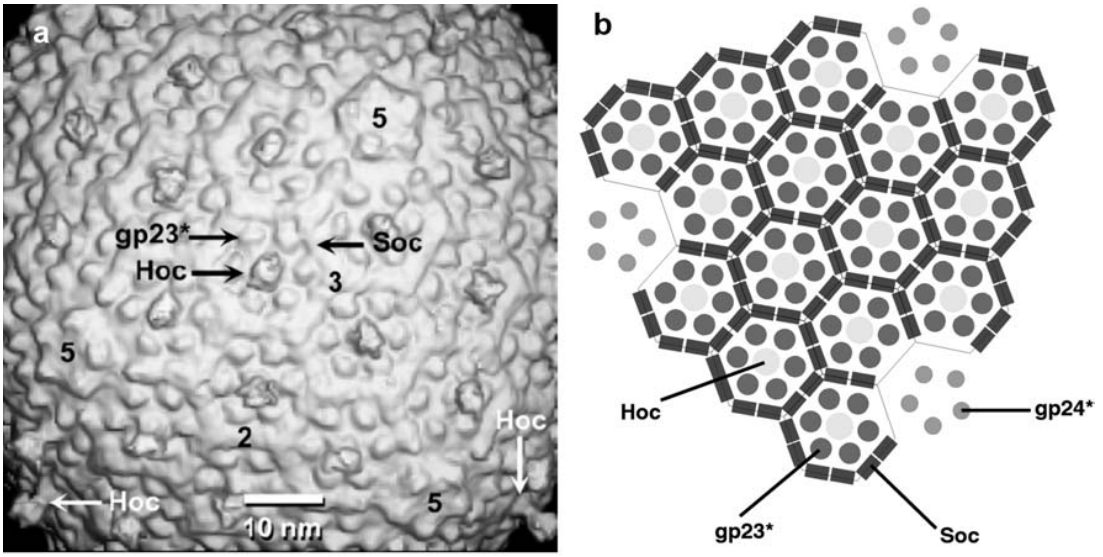

Figure 4. (*a*) A view, approximately along a threefold axis of the T4 capsid icosahedron, showing the organization of the hexamers and pentamers and the location of the two-, three-, and fivefold axes that limit an asymmetric unit (labeled 2, 3, and 5, respectively). (*b*) Schematic representation of the view from *a* showing the distribution of the capsid protein subunits within the shell. One gp hoc molecule associates with each hexamer of gp23*. The three gp23* hexamers nearest the icosahedral threefold axis are each surrounded by 12 gp soc molecules. The gp23* hexamers adjacent to the gp24* pentamers are each surrounded by only 10 gp soc molecules. Gp soc molecules are absent at the gp24*-gp23*interface. (Reprinted with permission from Olson et al. [20]. Copyright 2001, Academic Press.)

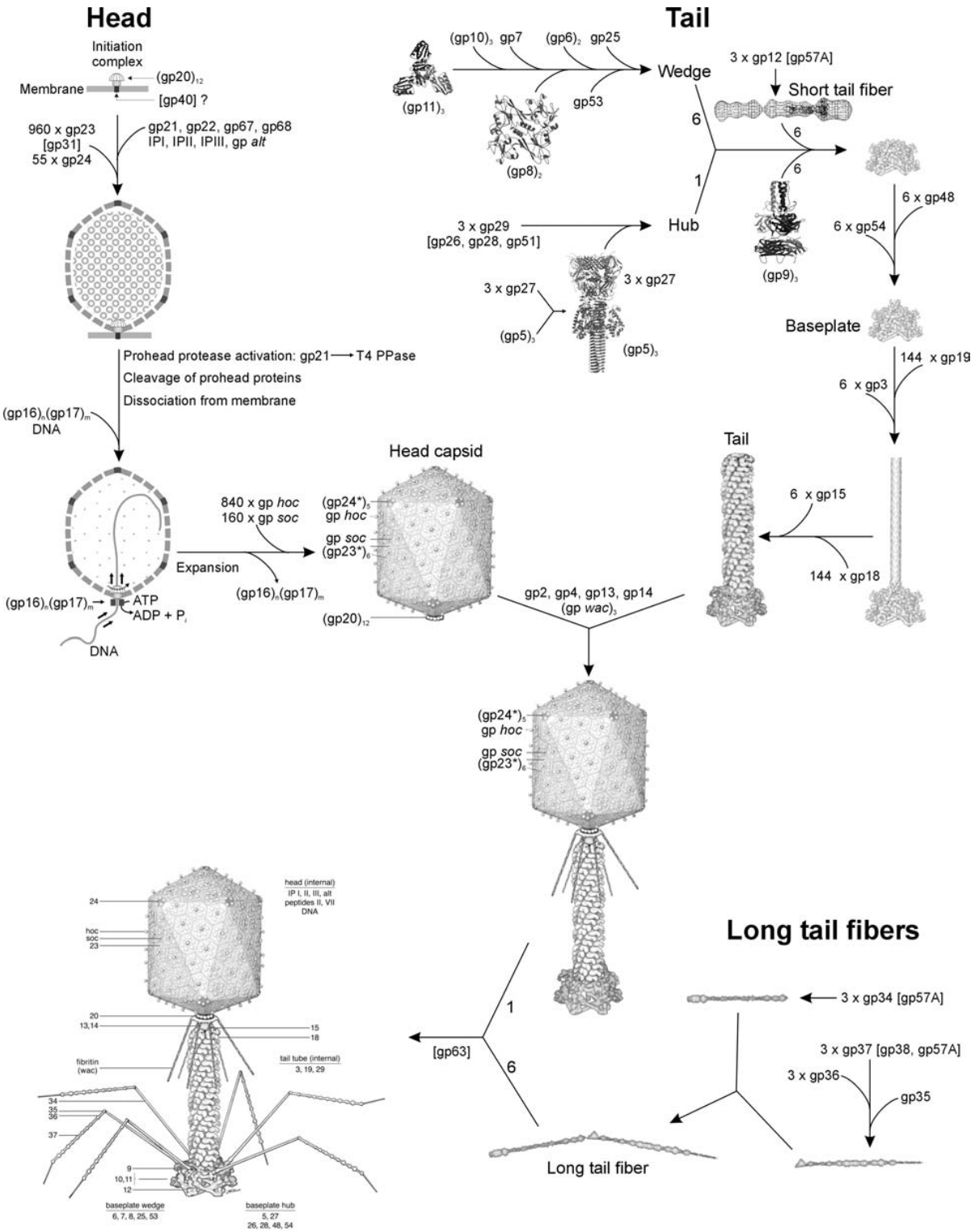

Figure 5. Morphogenesis of the bacteriophage T4 virion. The overall assembly pathway can be divided into three independent stages: head, tail, and long tail fiber assembly. The chaperonines and catalytic proteins are indicated in brackets near the protein, or assembly step, that requires the chaperonine. Known protein stoichiometries are given as subscripts. Crystal structures of structural proteins are shown as ribbon drawings.

tach to the gp20-gp40 complex and form a scaffold, which is then coated by a shell of gp23 and gp24. The dimensions of this prohead are about 15–20% smaller than those of the mature head. The proteins gp68, IPI, IPII, IPIII, and gp alt are not required for assembly, but rather help to eliminate incorrectly assembled intermediates that form dead-end products of maturation.

The scaffold and shell proteins in the fully assembled proheads undergo proteolytic cleavage by gp21, which is converted into its active form, called the prohead protease (T4PPase), by slow self-cleavage [26, 28–31]. The portal protein, gp20, similar to the portal vertex proteins of other tailed phages, is not cleaved during this process. The activated T4PPase cleaves the amino termini of gp23, gp24, IPI, IPII, IPIII, and gp alt and extensively digests gp22, gp21, gp67, and gp68 (reviewed in Black et al. [13]). All peptide fragments, except for peptide II and peptide VII derived from gp67 and gp22, respectively, are expelled from the prohead, thus providing free space to accommodate the genomic DNA during packaging.

Gp21 performs self-cleavage only when incorporated into the assembled prohead, suggesting that an exact 3D arrangement of several gp21 subunits and, possibly, other prohead proteins is required for the activation of gp21. Post-assembly self-cleavage of the structural proteins is a common feature of many viruses. For example, in picornaviruses, VP0 is cleaved to produce VP2 and VP4, and in retroviruses, the viral protease cleaves itself off the Gag polyprotein [reviewed in ref. 32].

The folding of gp23 is controlled by the GroEL chaperone working in concert with the phage-encoded chaperonine gp31 (table 2), which substitutes GroES in the infected cells [reviewed in ref. 33]. Despite low sequence identity (about 14%), gp31 and GroES have similar folds, form donut-shaped heptamers, and serve as a cap for the GroEL protein-folding chamber [34]. The volume of the GroEL/GroES chamber is insufficient to accommodate a gp23 monomer and, hence, gp23 requires gp31, which provides a folding chamber of a greater volume.

Table 2. T4-encoded chaperonines necessary for phage morphogenesis [13, 15, 59, 67–69, 94].

Gene	Mass (kDa)	Proteins that require the chaperonine
57A	5.7	gp12, gp34, gp37
26	23.9	activates gp29
28	17.3	activates gp29
51	29.3	activates gp29
31	12.0	gp23
38	22.3	gp37
40	13.2	activates gp20
wac	51.7	LTF to baseplate attachment
63	43.5	LTF to baseplate attachment

LTF, long tail fiber.

DNA packaging

The proteolytically processed proheads are released from the cytoplasmic membrane for DNA packaging. The T4 DNA substrate is a long, branched concatemer created by multiple rounds of homologous recombination between the ends of several genomic DNA molecules synthesized immediately after the infection has occurred. Upon recombination, a branch in the concatemer can contain up to 20 phage genomes along its length. The T4 endonuclease VII, encoded by gene 49, cleaves the dsDNA concatemer at the branch points [35], thus creating small regions of single-stranded DNA (ssDNA). These regions are recognized by gp17 [36], which is the large subunit of the gp16-gp17 hetero-oligomeric complex called the terminase [37]. Gp17 digests these ssDNA regions, but remains associated with the rest of the DNA. The terminase complex bound to DNA is then transported to the portal vertex of the prohead where the gp17 ATPase interacts with the gp20 portal protein [38]. The packaging proceeds until the head is full, after which the terminase cuts the capsid free from the rest of the DNA substrate. The process of packaging requires ATPase activity of gp17 [39, 40], which is greatly facilitated by gp16 [41].

Tailed phages and herpes simplex viruses package DNA into a preformed prohead in a similar fashion. The packaging apparatus has been proposed to represent a rotary motor powered by a virally encoded ATPase via ATP hydrolysis [42, 43]. The DNA is a movable central spindle of the motor, surrounded by a dodecameric portal protein serving as a ball race between the DNA spindle and the fivefold symmetric capsid vertex, to which the ATPase complex is attached. During packaging, the ATPase powers rotation of the portal protein, which causes translocation of the helical DNA molecule into the capsid. Although the sequence homology between the connector proteins from different tailed phages is low (less than 20%), they all have a similar cone-shaped dodecameric structure, and function similarly (fig. 6) [21, 43–46]. Furthermore, the connectors from phages ϕ29 (19.3-kbp genome) and λ (48.5-kbp genome) are interchangeable [47].

Similar to other dsDNA tailed phages, such as λ, HK97, T3, T7, and P22, initiation of DNA packaging in T4 causes prohead expansion [48, 49]. Upon initiation of DNA packaging, the hexagonal lattice of the T4 prohead expands from a 117-Å to a 140-Å repeat distance between the gp23* hexamer centers, increasing the capsid volume by 50% [19]. The expansion involves rotation of the gp23* hexamers [50] and their partial refolding [51]. This transformation stabilizes the capsid structure and creates binding sites for gp hoc and gp soc [24].

Mutants with altered lengths of the capsid cylindrical midsection are capable of DNA packaging [52–54]. The length of the packaged DNA is proportional to the volume of the head: the isometric heads contain only about

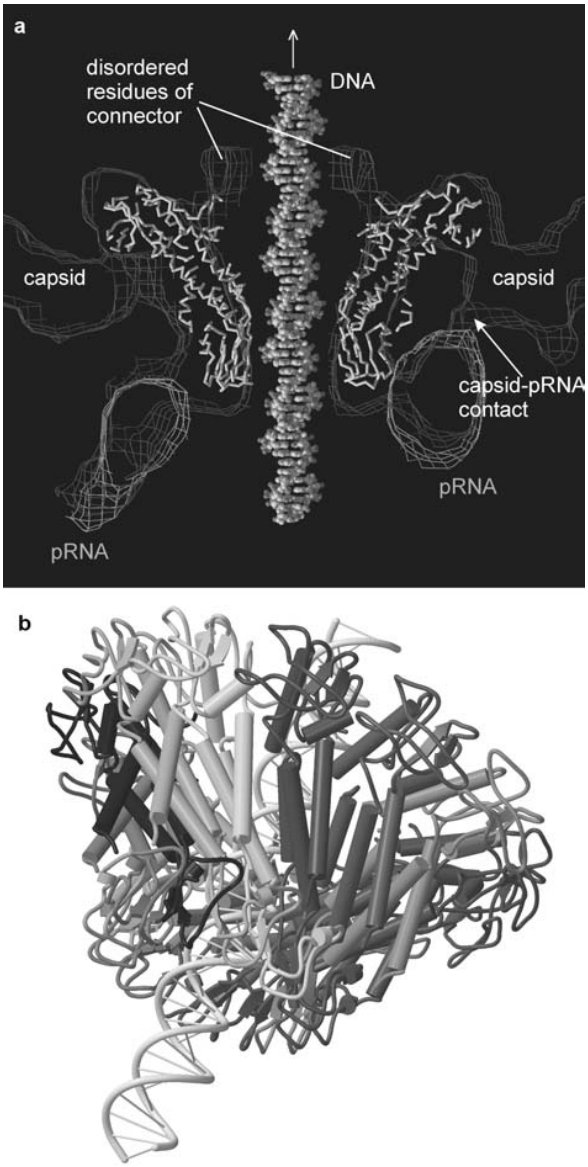

Figure 6. Structure of the dsDNA tailed phage ϕ29 portal vertex. (*a*) Cross-section of the cryoEM prohead density (gray mesh) fitted with the C_α backbone of the ϕ29 portal protein, called the head-tail connector (solid lighter gray), and the difference cryoEM map of the structural prohead RNA (pRNA) surrounding the portal vertex (light-gray mesh). Shown also is a DNA molecule passing through the central channel of the connector. The viral ATPase, which powers the DNA-packaging process, binds to the pRNA during packaging. (Reprinted with permission from Simpson et al. [43]. Copyright 2000, Nature Publishing Group.) (*b*) Structure of the ϕ29 connector, which is homologous to the T4 portal protein, gp20. Helices are shown as cylinders. The 12 monomers and the DNA, passing through the central pore, are colored in different shades of gray. (Reprinted with permission from Simpson et al. [97]. Copyright 2001, International Union of Crystallographers.)

70% of the genome, whereas the giant heads can contain more than a dozen of the genomic sequences repeated along a single dsDNA molecule. The density of packaged DNA is similar in all head types [13] and, therefore, the termination of packaging is regulated by the stress applied during DNA packaging on the portal complex and/or the entire shell. The packaged DNA is probably wound in a tight toroidal bundle [55] whose axis is perpendicular to the head length. In phage T7, however, the axis of the bundle is along the phage length [56]. The toroid consists of DNA layers separated by 24 Å in both T4 and T7 [20, 56].

Upon completion of DNA packaging, the gp16-gp17 terminase complex dissociates from the head. The head maturation is finalized by attachment of gp13, gp14, gp2, and gp4 to the portal vertex. These proteins are necessary for subsequent attachment of the independently assembled tail and fibers to produce the infectious virus particles. Since the tails do not attach to the empty but otherwise mature heads, a DNA-mediated interaction is involved in the joining process. In T4, as is the case for phages λ and T5 [57], one end of the packaged DNA might descend into the tail.

The tail, fibers, and infection process

Tail structure and morphogenesis

Phages from the *Myoviridae* family have exceptionally complex, contractile tails. Bacteriophage T4 devotes 25 kbp of its genome to tail assembly, which is compara-

Table 3. T4 baseplate and tail tube proteins in order of appearance in the T4 genetic map (modified from Coombs and Arisaka [14]).

Gene	Mass (kDa)	Copy number	Location
3	19.7	6	tail tube terminator
53	23.0	6	wedge
5	63.7	3	hub
6	74.4	12	wedge
7	119.2	6	wedge-vertex
8	38.0	12	wedge
9	31.0	18	wedge-vertex
10	66.2	18	wedge-pin
11	23.7	18	wedge-pin
12	55.3	18	STF
15	31.4	6	tail terminator
18	71.2	144	tail sheath
19	18.5	144	tail tube
25	15.1	6	wedge
27	44.4	3	hub
29	64.4	6	tail tube
48	39.7	6	baseplate
54	35.0	6	baseplate
td	33.1	3	hub?
frd	21.7	6	wedge?

STF, short tail fiber.

ble with the size of the entire adenovirus genome (36 kbp). Products of at least 22 genes are involved in tail assembly (table 3), which include a phage-encoded chaperone that participates in folding of the long and short tail fibers (table 2) [58–60].

The bacteriophage T4 tail is composed of two concentric protein cylinders, at one end of which is the baseplate and fibers (fig. 1) [6]. The inner cylinder, called the tail tube, is built of 144 copies of gp19 [61, 62]. The tail tube has a 40 Å-diameter channel for DNA passage from the head to the infected cell [5]. The outer cylinder, called the tail sheath, tightly envelopes the 90 Å-diameter tail tube and has a width of about 210 Å. It is composed of 144 copies of gp18 [5, 61, 63]. The subunits comprising each cylinder form a six-start helix with a pitch of 41 Å and a right-handed twist angle of 17°. The helix has a length of 984 Å and contains 24 repeats [5, 63].

During infection, the phage recognizes an *E. coli* bacterium using its long tail fibers (LTFs) connected to the baseplate. The phage then anchors the baseplate to the lipopolysaccharide cell surface receptors using the short tail fibers (STF), which are initially assembled under the baseplate. This event triggers a hexagon-to-star conformational change in the baseplate [6] and causes an irreversible contraction of the tail sheath [64], releasing about 25 kcal/mol of energy per gp18 monomer [65]. During this process, the gp18 hexamers flatten, rotate, and expand radially, resulting in a decrease of their thickness by 26 Å and an increase of the twist angle by 15°. The contracted tail sheath has a length of only 360 Å and a width of 270 Å [66]. The tail tube does not change its length during sheath contraction. As a result, almost half of the tube protrudes out of the contracted tail sheath and the baseplate.

The sheath can be caused to contract by exposing the phage to 3 M urea. Nevertheless, the DNA is not released until the tail tube tip binds to a cytoplasmic membrane receptor common to enteric bacteria, suggesting that tail contraction does not cause the release of DNA [8]. The interaction of the tail tube tip with the cytoplasmic membrane involves creation of a channel for DNA passage. During DNA transfer from the capsid into the cell, the membrane remains virtually undamaged since the transfer requires a proton motive force across the membrane [8].

The assembly pathway of the bacteriophage T4 tail (fig. 5) is regulated by ordered sequential interactions of proteins rather than sequential gene expression [67–75]. The baseplate, a remarkably complex multiprotein structure, is assembled first. It is composed of about 150 subunits of at least 16 different gene products, many of which are oligomeric (table 3) (reviewed in Coombs and Arisaka [14]). These proteins form six independently assembled wedges that join together around the central hub with the help of the trimeric proteins $(gp9)_3$ [76] and $(gp12)_3$ [77]. Each wedge is assembled by sequential interactions of the seven protein oligomers: $(gp11)_3$ [78], $(gp10)_3$ [75], gp7, $(gp8)_2$ [79], $(gp6)_2$, gp53, and gp25. The baseplate hub is formed by $(gp5)_3$, $(gp27)_3$ [80], gp29 [81] and, probably, gp28 [82]. The assembly of the baseplate is completed with the attachment of six copies of gp48 and six copies of gp54 [72] to the external interface between the wedges and the hub. The latter proteins serve as a starting point for polymerization of gp19 to form the tail tube [83], which is terminated with gp3 [84, 85]. The tail tube serves as a scaffold for polymerization of the tail sheath around it. During this process, gp18 stores energy in its conformation (possibly by ATP hydrolysis [86]), making the non-contracted T4 tail a stretched spring. The length of the tail tube is controlled by the ruler protein, gp29 [81], which also participates in assembly of the central part of the baseplate [69]. The length of the tail sheath is determined by the length of the tube. The assembly of the tail is completed by attachment of a gp15 hexamer to the last ring of the tail sheath [87].

CryoEM reconstruction of the baseplate-tail tube complex [80] shows that the baseplate is a dome-shaped object which is 270 Å high and 520 Å in diameter at its widest part (fig. 7). The hollow tail tube stems from the center of the baseplate. One of the most remarkable fea-

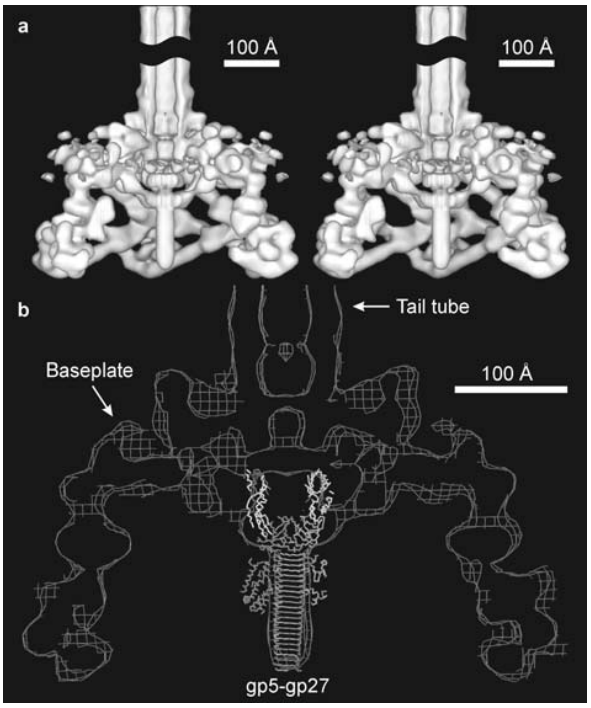

Figure 7. CryoEM reconstruction of the T4 baseplate-tail tube assembly. (*a*) Stereo view of the surface-shaded representation. The top quarter of the baseplate has been removed to visualize the internal features. (*b*) Cross-sectioned density fitted with the atomic structure of the gp5-gp27 complex. For clarity, the contour level of the surface-shaded figure in *a* is higher than the contour level of the cross-sectioned density in *b*. Thus, some of the density representing gp27 in *a* is missing compared to *b*. (Reprinted with permission from Kanamaru et al. [80]. Copyright 2002, Nature Publishing Group.)

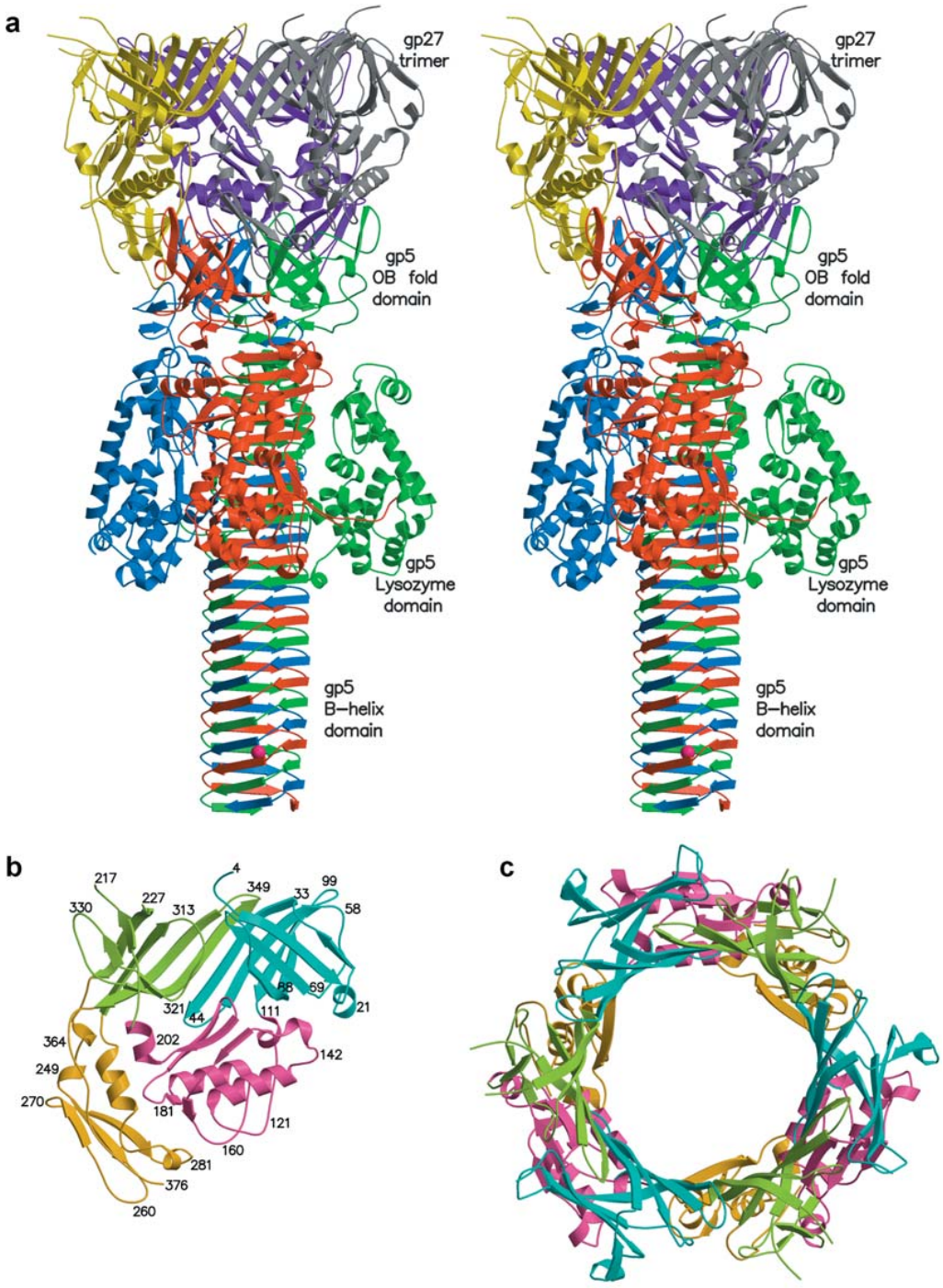

Figure 8. Structure of the gp5-gp27 complex. (*a*) Ribbon stereo diagram. The three gp5 monomers are colored red, green, and blue. The three gp27 monomers are colored yellow, gray, and purple. The K^+ ion within gp5C is shown in pink. The $(PO_4)^-$ is hidden behind the lysozyme domain. (*b*) The structure of the gp27 monomer with its four domains colored cyan, pink, light green, and gold along the polypeptide chain. (*c*) Top view of the gp27 cylinder shows that the cyan and green domains form a hexagonal torus. (Reprinted with permission from Kanamaru et al. [81]. Copyright 2002, Nature Publishing Group.)

tures of the baseplate is a 30-Å wide, 110-Å long spike, or needle, along the axis of the dome. The crystal structure of the gp5-gp27 complex (fig. 8) can be fitted into the baseplate map so that the needle density is occupied by the C-terminal domain of gp5 (fig. 7). The gp27 trimer forms a channel suitable for passage of a dsDNA and serves as an extension of the tail tube (figs 7, 8).

Gp5 consists of three domains: an N-terminal oligosaccharide binding-fold domain, the middle lysozyme domain, and the C-terminal triple *β*-helix domain (figs 8, 9) [80]. The gp5 lysozyme domain has 43% sequence identity [88] and a closely similar structure to the T4 lysozyme encoded by gene *e* (T4L) [89]. The active center residues in both proteins are the same, suggesting a common evolutionary origin. Gp5 undergoes a maturation cleavage between residues Ser351 and Ala352 (fig. 9), but both the resultant parts, the N-terminal part (gp5*) and the C-terminal part (gp5C), remain associated and are found in the phage particle [90]. Dissociation of the gp5C trimer from gp5* frees the gp5* substrate-binding sites [81] and increases the lysozyme activity of gp5* by at least tenfold [90] (fig. 9).

The T4 STF (table 4) is a gp12 trimer, which is attached to the baseplate via gp11 [78]. The STF is a 340 Å-long, club-shaped molecule, which has a narrowing in the middle of the shaft where it can bend by up to 90° [91]. This feature might be necessary to accommodate the folded fiber into the baseplate. Three polypeptide chains of gp12 run in register through the length of the club starting from the shaft end towards the club head end [77, 91]. During infection, the club heads (the C termini of gp12 molecules) bind to the core region of the lipopolysaccharide cell surface receptors [91], while the club shaft remains associated with the baseplate [91].

Both gp12 and gp5 contain remarkable right-handed, triple-stranded, *β*-helix domains, which are composed of three intertwined, in register protein chains. The triple-stranded *β*-helices in gp5 and gp12 are somewhat different to each other. The gp5 *β*-helix has a well-defined, eight-residue repeat with a common motif (**V**X**G**XXXXX) [88, 90], whereas the gp12 helix does not have a repeating sequence motif. Moreover, the strands in the gp12 helix vary slightly in length (five to seven residues per strand), although a repeat consensus of six residues can be established. The inside of the gp12 helix is hydrophobic, whereas the inside of the gp5 helix has hydrophobic, polar, and charged patches. In addition, on the inside of the gp5 helix there are more than 40 water molecules and two ions situated on the three-fold axis. The gp5 helix probably represents a mechanically firmer structure than the gp12 helix, making gp5 especially suitable as a needle for puncturing the host membrane.

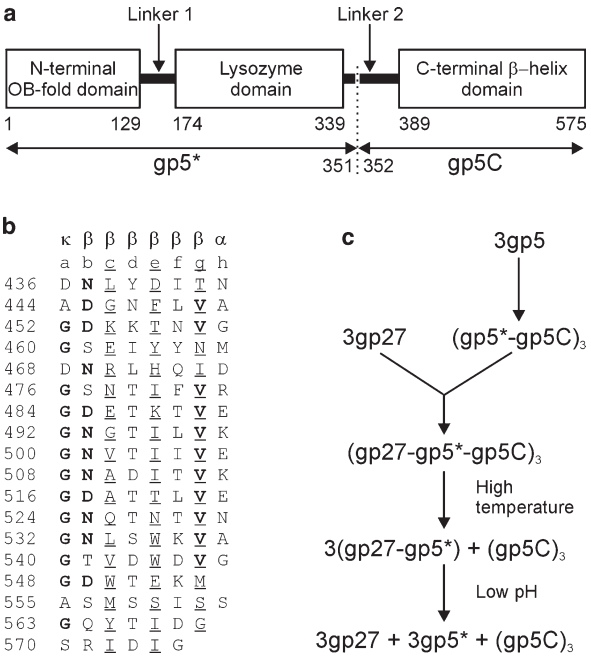

Figure 9. Assembly of the gp5-gp27 complex. (*a*) Domain organization within the gp5 monomer. The maturation cleavage is indicated by the dotted line. The three gp5 domains are shown as rectangles with the initial and last residue number indicated. (*b*) Alignment of the octapeptide units composing the intertwined part of the c-terminal *β*-helix domain of gp5. Conserved residues are in bold print; residues facing the inside are underlined. The main chain dihedral angle configuration of each residue in the octapeptide is indicated at the top by κ (kink), β (sheet), or α (helix). (*c*) Assembly of gp5 and gp27 into the hub and needle of the baseplate. (Reprinted with permission from Kanamaru et al. [80]. Copyright 2002, Nature Publishing Group.)

Long tail fibers

The LTFs (table 4) of bacteriophage T4 are adsorption devices and environmental sensors [8]. They are connected to the baseplate via gp9 and gp7 [76, 84]. The fibers are about 1450 Å long and only 40 Å in diameter. Each fiber consists of the rigid proximal and distal parts connected by a hinge region [7, 15]. The gp34 trimer forms the proximal part, whereas the distal part is composed of the trimeric gp36 and gp37 and the monomeric gp35 (fig. 10) [7, 15]. The N termini of the gp34 trimer form the baseplate-binding bulge, whereas its C termini, gp35, and a part of the gp36 trimer participate in formation of the hinge. The gp36 trimer comprises about 13 nm of the distal part of the LTF and interacts with the gp34 trimer, which forms the rest of the fiber (fig. 10). The fiber is composed of a repeating motif, common to gp34, gp37, and gp12 (STF), with intervening sequences of different lengths (fig. 10). The C-terminal regions of gp37 and gp12 are homologous, presumably because both function to bind lipopolysaccharides [7, 93]. Two phage-encoded chaperones, gp57A and gp38, are required for assembly

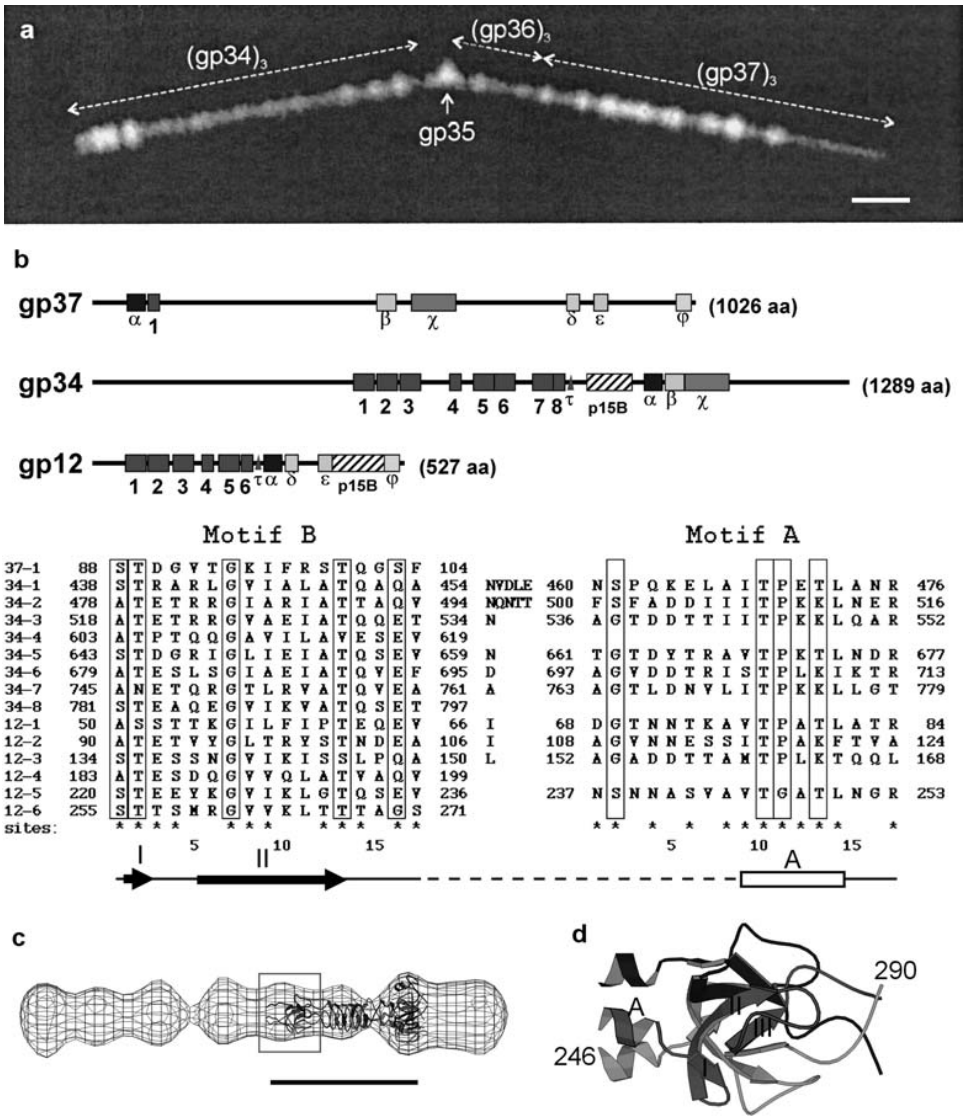

Figure 10. Domain organization of the long and short tail fibers. (*a*) The phage T4 LTF. The proteins comprising the fiber and their oligomerization states are indicated. The baseplate-binding bulge of the fiber is on the left and the receptor recognition tip is on the right. The bar represents 10 nm. (*b*) Repeat segments and homologous regions shared among the T4 tail fiber proteins. Linear representations of the amino acid sequences (total number of amino acid residues in each protein is indicated in parentheses) of gp37, gp34, and gp12 are shown. The regions of homology are boxed and labeled with Greek letters. p15B indicates regions of homology shared with the plasmid p15B of *E. coli* [98]. The numbered boxes correspond to occurrences of the repeat motifs called 'A' and 'B,' the sequences of which are listed below. Each repeat is labeled with the gene product number followed by the corresponding repeat number within that protein (i.e. the sequence labeled '34-1' corresponds to the first boxed repeat within gp34). The positions of the start and stop residues of the A and B motifs are indicated. Intervening sequences, if present, are included. Highly conserved residues are boxed, and the residue positions detected as key sites by the iterative sampling algorithm of Lawrence et al. [99] are indicated by an asterisk. The secondary structure elements derived from the gp12 fragment crystal structure are shown in register with the sequence below the alignment. The open box labeled 'A' is the α helix, the arrows 'I' and 'II' are the two β strands, and the dashed line represents the region of the polypeptide chain that was disordered in the crystal structure. The bar represents 100 Å. (Reprinted with permission from Cerritelli et al. [7]. Copyright 1996, Elsevier Science.) (*c*) Crystal structure of the gp12 STF fragment fitted into a cryoEM reconstruction of the whole fiber. The conserved domain, consisting of the sequence labeled as '12-6' in *b* is highlighted with the gray box. (*d*) A ribbon representation of the conserved domain. The first and last residues are numbered. The secondary-structure elements are named as in *b*. (Reprinted with permission from van Raaij et al. [77]. Copyright 2001, Elsevier Science.)

Table 4. T4 fibers.

Gene	Mass (kDa)	Copy number	Fiber	Location
12	55.3	3	STF	baseplate
34	140.0	3	LTF	proximal part, connected to the baseplate
35	30.0	1	LTF	hinge region
36	23.0	3	LTF	distal part, hinge connection
37	109.0	3	LTF	distal part, receptor recognition tip
wac	51.9	3	head whisker	head-tail joining region

The copy number is given per fiber. There are six fibers of each type per virion [7, 15, 91, 94].

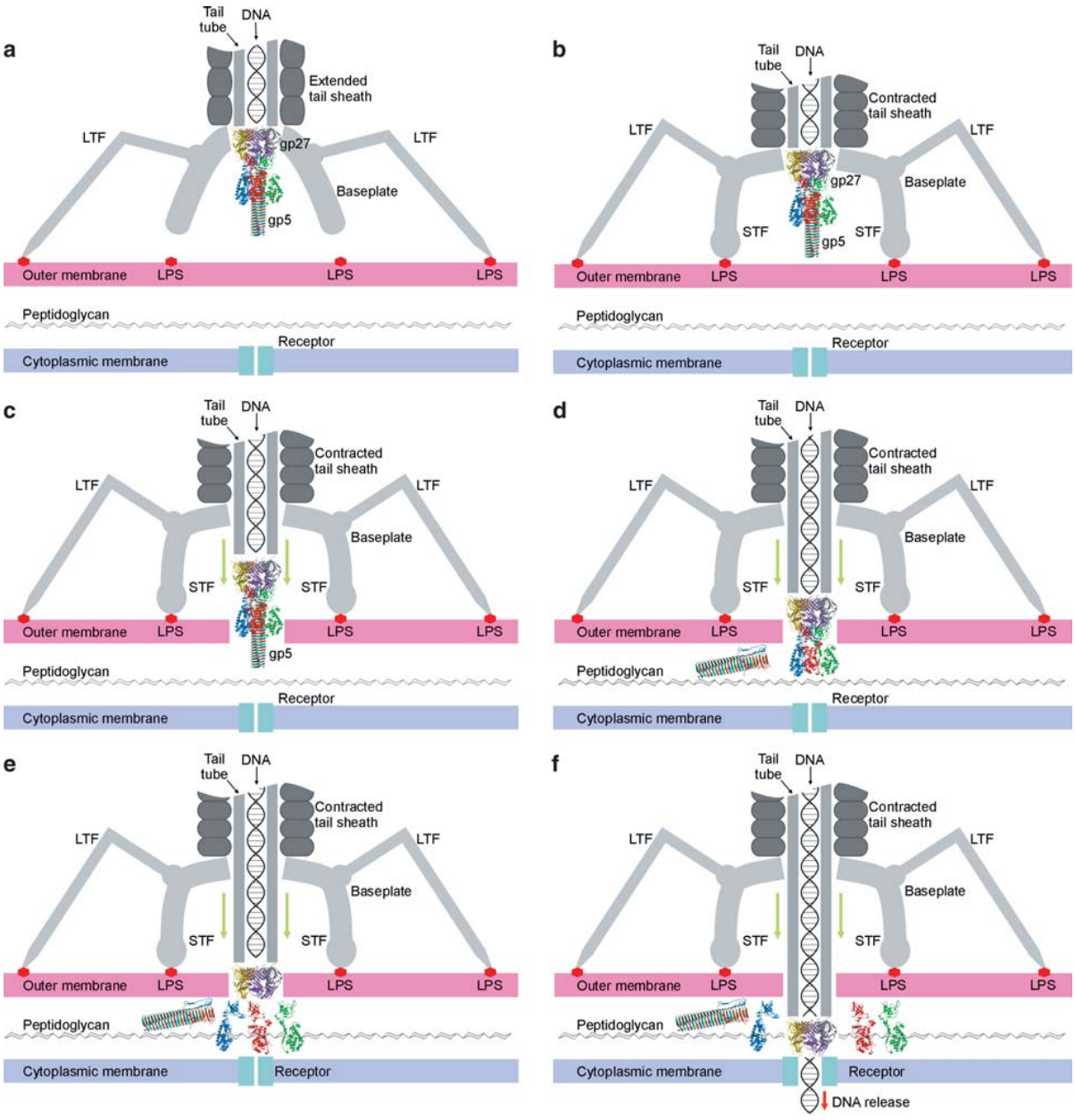

Figure 11. Infection process. (*a*) T4 phage recognizes the *E. coli* LPS molecules using the LTFs. (*b*) The phage attaches the baseplate to the cell surface initiating contraction of the tail sheath. (*c*) Tail contraction causes the gp5 needle to puncture the outer cell membrane. (*d*) Gp5C dissociates from the tail tube, thus activating the three lysozyme domains. (*e*) The lysozyme domains create an opening in the peptidoglycan layer. (*f*) Gp27 associates with a receptor on the inner membrane, which initiates release of DNA into the cytoplasm.

of the LTFs (fig. 5) and another two, gp63 and gp *wac* [94], for attachment of the fibers to the baseplate (table 2). Gp57A is also required for solubility and trimerization of gp12 in vitro and in vivo [59].

Infection process

The structural and biochemical results lead to a probable mechanism of infection [8], which is likely related to the infection processes in many other viruses (fig. 11). The T4 phage initiates infection of an *E. coli* bacterium by recognizing the lipopolysaccharide cell surface receptors with the distal ends of its LTFs. The recognition signal is then transmitted through the LTFs to the baseplate attachment protein, gp9, and then to the baseplate itself. Subsequently, the STFs unravel from underneath the baseplate and bind irreversibly to the lipopolysaccharide cell surface receptors, thus securely anchoring the baseplate to the cell membrane. The baseplate changes its conformation from hexagonal to star-shaped, causing contraction of the tail sheath. The contracted tail sheath drives the head closer to the cell surface and, therefore, exerts a force onto the tail tube directed toward the cell membrane. This force is transmitted through the gp27 cylinder and the N-terminal domain of gp5 to the β-helix needle, causing the latter to puncture the outer membrane of the cell [80]. As the tail sheath contraction progresses, the β-helix needle spans the entire 40 Å width of the outer membrane, thereby enlarging the pore in the membrane. Subsequently, when the β-helix needle comes into contact with the periplasmic peptidoglycan layer, it dissociates from the tip of the tube, thus activating the lysozyme domain of gp5 [90]. The latter digests the cell wall, allowing penetration of the tail tube to the inner membrane [92]. The gp27 trimer, forming the tip of the tail tube, probably interacts with a specific receptor molecule on the cytoplasmic membrane to initiate release of DNA from the phage head through the tail tube into the host cell.

Acknowledgements. We are grateful to V. Kostyuchenko for many helpful discussions and to S. Wilder and C. Towell for help in preparation of the manuscript. This work was supported by a National Science Foundation grant to M. G. R. and a Howard Hughes Medical Institute grant to V. V. M.

1 Sanger F., Air G. M., Barrell B. G., Brown N. L., Coulson A. R., Fiddes J. C. et al. (1977) Nucleotide sequence of bacteriophage ϕX174 DNA. Nature **265:** 687–695
2 Mesyanzhinov V. V., Robben J., Grymonpreq B., Kostyuchenko V. A., Bourkaltseva M. V., Sykilinda N. N. et al. (2002) The genome of bacteriophage ϕKZ of *Pseudomonas aeruginosa*. J. Mol. Biol. **317:** 1–19
3 Kutter E. M., Guttmann B., Mosig G. and Rüger W. (1990) T4 genomic map. In: Genomic Maps, pp. 1–27, O'Brien S. J. (ed.), Cold Spring Harbor Laboratory Press, Cold Spring Harbor, N. Y.
4 Baschong W., Aebi U., Baschong-Preschianotto C., Dubochet J., Landmann L., Kellenberger E. et al. (1988) Head structure of bacteriophages T2 and T4. J. Ultrastruct. Mol. Struct. Res. **99:** 189–202
5 DeRosier D. J. and Klug A. (1968) Reconstruction of three dimensional structures from electron micrographs. Nature **217:** 130–134
6 Crowther R. A., Lenk E. V., Kikuchi Y. and King J. (1977) Molecular reorganization in the hexagon to star transition of the baseplate of bacteriophage T4. J. Mol. Biol. **116:** 489–523
7 Cerritelli M. E., Wall J. S., Simon M. N., Conway J. F. and Steven A. C. (1996) Stoichiometry and domainal organization of the long tail-fiber of bacteriophage T4: a hinged viral adhesin. J. Mol. Biol. **260:** 767–780
8 Goldberg E., Grinius L. and Letellier L. (1994) Recognition, attachment, and injection. In: Molecular Biology of Bacteriophage T4, pp. 347–356, Karam J. D. (ed.), American Society for Microbiology, Washington, D. C.
9 Ackerman H.-W. and Krisch H. M. (1997) A catalogue of T4-type bacteriophages. Arch. Virol. **142:** 2329–2345
10 Fuller N. J., Wilson W. H., Joint I. R. and Mann N. H. (1998) Occurrence of a sequence in marine cyanophages similar to that of T4 g20 and its application to PCR-based detection and quantification techniques. Appl. Environ. Microbiol. **64:** 2051–2060
11 Takeda S., Sasaki T., Ritani A., Howe M. M. and Arisaka F. (1998) Discovery of the tail tube gene of bacteriophage Mu and sequence analysis of the sheath and tube genes. Biochim. Biophys. Acta **1399:** 88–92
12 Hendrix R. W., Smith M. C. M., Burns R. N., Ford M. E. and Hatfull G. F. (1999) Evolutionary relationships among diverse bacteriophages and prophages: all the world's a phage. Proc. Natl. Acad. Sci. USA **96:** 2192–2197
13 Black L. W., Showe M. K. and Steven A. C. (1994) Morphogenesis of the T4 head. In: Molecular Biology of Bacteriophage T4, pp. 218–258, Karam J. D. (ed.), American Society for Microbiology, Washington, D. C.
14 Coombs D. H. and Arisaka F. (1994) T4 tail structure and function. In: Molecular Biology of Bacteriophage T4, pp. 259–281, Karam J. D. (ed.), American Society for Microbiology, Washington, D. C.
15 Wood W. B., Eiserling F. A. and Crowther R. A. (1994) Long tail fibers: genes, proteins, structure, and assembly. In: Molecular Biology of Bacteriophage T4, pp. 282–290, Karam J. D. (ed.), American Society for Microbiology, Washington, D. C.
16 Eiserling F. A. and Black L. W. (1994) Pathways in T4 morphogenesis. In: Molecular Biology of Bacteriophage T4, pp. 209–212, Karam J. D. (ed.), American Society for Microbiology, Washington, D. C.
17 Baschong W., Baschong-Preschianotto C., Engel A., Kellenberger E., Lustig A., Reichelt R. et al. (1991) Mass analysis of bacteriophage T4 proheads and mature heads by scanning transmission electron microscopy and hydrodynamic measurements. J. Struct. Biol. **106:** 93–101
18 Moody M. F. (1999) Geometry of phage head construction. J. Mol. Biol. **293:** 401–433
19 Aebi U., Bijlenga R., Broek J. van der, Broek R. van der, Eiserling F., Kellenberger C. et al. (1974) The transformation of τ particles into T4 heads. II. Transformations of the surface lattice and related observations on form determination. J. Supramol. Struct. **2:** 253–275
20 Olson N. H., Gingery M., Eiserling F. A. and Baker T. S. (2001) The structure of isometric capsids of bacteriophage T4. Virology **279:** 385–391
21 Driedonks R. A., Engel A., tenHeggeler B. and van Driel R. (1981) Gene *20* product of bacteriophage T4: its purification and structure. J. Mol. Biol. **152:** 641–662
22 Ishii T. and Yanagida M. (1977) The two dispensable structural proteins (soc and hoc) of the T4 phage capsid: their properties, isolation, and characterization of defective mutants, and their

binding with the defective heads in vitro. J. Mol. Biol. **109:** 487–514
23 Ishii T., Yamaguchi Y. and Yanagida M. (1978) Binding of the structural protein Soc to the head shell of bacteriophage T4. J. Mol. Biol. **120:** 533–544
24 Steven A. C., Greenstone H. L., Booy F. P., Black L. W. and Ross P. D. (1992) Conformational changes of a viral capsid protein: thermodynamic rationale for proteolytic regulation of bacteriophage T4 capsid expansion, co-operativity, and superstabilization by Soc binding. J. Mol. Biol. **228:** 870–884
25 Iwasaki K., Trus B. L., Wingfield P. T., Cheng N., Campusano G., Rao V. B. et al. (2000) Molecular architecture of bacteriophage T4 capsid: vertex structure and bimodal binding of the stabilizing accessory protein, Soc. Virology **271:** 321–333
26 Laemmli U. K. (1970) Cleavage of structural proteins during the assembly of the head of bacteriophage T4. Nature **227:** 680–685
27 Hsiao C. L. and Black L. W. (1978) Head morphogenesis of bacteriophage T4. II. The role of gene 40 in initiating prehead assembly. Virology **91:** 15–25
28 Laemmli U. K., Amos L. A. and Klug A. (1976) Correlation between structural transformation and cleavage of the major head protein of T4 bacteriophage. Cell **7:** 191–203
29 Steven A. C., Couture E., Aebi U. and Showe M. K. (1976) Structure of T4 polyheads. II. A pathway of polyhead transformations as a model for T4 capsid maturation. J. Mol. Biol. **106:** 187–221
30 Showe M. K., Isobe E. and Onorato L. (1976) Bacteriophage T4 prehead proteinase. I. Purification and properties of a bacteriophage enzyme which cleaves the capsid precursor proteins. J. Mol. Biol. **107:** 35–54
31 Showe M. K., Isobe E. and Onorato L. (1976) Bacteriophage T4 prehead proteinase. II. Its cleavage from the product of gene 21 and regulation in phage-infected cells. J. Mol. Biol. **107:** 55–69
32 Flint S. J., Enquist L. W., Krug R. M., Racaniello V. R. and Skalka A. M. (2000) Assembly, exit and maturation of progeny viruses. In: Principles of Virology: Molecular Biology, Pathogenesis, and Control, pp. 438–476, Flint S. J. et al. (eds), American Society for Microbiology, Washington, D. C.
33 Richardson A., Landry S. J. and Georgopoulos C. (1998) The ins and outs of a molecular chaperone machine. Trends Biochem. Sci. **23:** 138–143
34 Hunt J. F., Vies S. M. van der, Henry L. and Deisenhofer J. (1997) Structural adaptations in the specialized bacteriophage T4 co-chaperonin Gp31 expand the size of the Anfinsen cage. Cell **90:** 361–371
35 Mizuuchi K., Kemper B., Hays J. and Weisberg R. A. (1982) T4 endonuclease VII cleaves Holliday structures. Cell **29:** 257–265
36 Franklin J., Haseltine D., Davenport L. and Mosig G. (1998) The largest (70 kDa) product of the bacteriophage T4 DNA terminase gene 17 binds to single-stranded DNA segments and digests them towards junctions with double-stranded DNA. J. Mol. Biol. **277:** 541–557
37 Black L. W. (1989) DNA packaging in dsDNA bacteriophages. Annu. Rev. Microbiol. **43:** 267–292
38 Hsiao C. L. and Black L. W. (1977) DNA packaging and the pathway of bacteriophage T4 head assembly. Proc. Natl. Acad. Sci. USA **74:** 3652–3656
39 Bhattacharyya S. P. and Rao V. B. (1993) A novel terminase activity associated with the DNA packaging protein gp17 of bacteriophage T4. Virology **196:** 34–44
40 Leffers G. and Rao V. B. (2000) Biochemical characterization of an ATPase activity associated with the large packaging subunit gp17 from bacteriophage T4. J. Biol. Chem. **275:** 37127–37136
41 Rao V. B. and Black L. W. (1988) Cloning, overexpression and purification of the terminase proteins gp16 and gp17 of bacteriophage T4. Construction of a defined in vitro DNA packaging system using purified terminase proteins. J. Mol. Biol. **200:** 475–488
42 Hendrix R. W. (1978) Symmetry mismatch and DNA packaging in large bacteriophages. Proc. Natl. Acad. Sci. USA **75:** 4779–4783
43 Simpson A. A., Tao Y., Leiman P. G., Badasso M. O., He Y., Jardine P. J. et al. (2000) Structure of the bacteriophage ϕ29 DNA packaging motor. Nature **408:** 745–750
44 Kochan J., Carrascosa J. L. and Murialdo H. (1984) Bacteriophage lambda preconnectors. Purification and structure. J. Mol. Biol. **174:** 433–447
45 Valpuesta J. M., Serrano M., Donate L. E., Herranz L. and Carrascosa J. L. (1992) DNA conformational change induced by the bacteriophage ϕ29 connector. Nucleic Acids Res. **20:** 5549–5554
46 Lurz R., Orlova E. V., Gunther D., Dube P., Droge A., Weise F. et al. (2001) Structural organisation of the head-to-tail interface of a bacterial virus. J. Mol. Biol. **310:** 1027–1037
47 Donate L. E., Murialdo H. and Carrascosa J. L. (1990) Production of lambda-phi 29 phage chimeras. Virology **179:** 936–940
48 Jardine P. J. and Coombs D. H. (1998) Capsid expansion follows the initiation of DNA packaging in bacteriophage T4. J. Mol. Biol. **284:** 661–672
49 Jardine P. J., McCormick M. C., Lutze-Wallace C. and Coombs D. H. (1998) The bacteriophage T4 DNA packaging apparatus targets the unexpanded prohead. J. Mol. Biol. **284:** 647–659
50 Steven A. C. and Carrascosa J. L. (1979) Proteolytic cleavage and structural transformation: their relationship in bacteriophage T4 capsid maturation. J. Supramol. Struct. **10:** 1–11
51 Steven A. C., Bauer A. C., Bisher M. E., Robey F. A. and Black L. W. (1991) The maturation-dependent conformational change of phage T4 capsid involves the translocation of specific epitopes between the inner and the outer capsid surfaces. J. Struct. Biol. **106:** 221–236
52 Eiserling F. A., Geiduschek E. P., Epstein R. H. and Metter E. J. (1970) Capsid size and deoxyribonucleic acid length: the petite variant of bacteriophage T4. J. Virol. **6:** 865–876
53 Uhlenhopp E. L., Zimm B. H. and Cummings D. J. (1974) Structural aberrations in T-even bacteriophage. VI. Molecular weight of DNA from giant heads. J. Mol. Biol. **89:** 689–702
54 Lane L. C., Serwer P., Hayes S. J. and Eiserling F. A. (1990) Quantized viral DNA packaging revealed by rotating gel electrophoresis. Virology **174:** 472–478
55 Earnshaw W. C. and Harrison S. C. (1977) DNA arrangement in isometric phage heads. Nature **268:** 598–602
56 Cerritelli M. E., Cheng N., Rosenberg A. H., McPherson C. E., Booy F. P. and Steven A. C. (1997) Encapsidated conformation of bacteriophage T7 DNA. Cell **91:** 271–280
57 Saigo K. (1975) Tail-DNA connection and chromosome structure in bacteriophage T5. Virology **68:** 154–165
58 King J. and Laemmli U. K. (1971) Polypeptides of the tail fibres of bacteriophage T4. J. Mol. Biol. **62:** 465–477
59 Matsui T., Griniuviené B., Goldberg E., Tsugita A., Tanaka N. and Arisaka F. (1997) Isolation and characterization of a molecular chaperone, gp57A, of bacteriophage T4. J. Bacteriol. **179:** 1846–1851
60 Burda M. R. and Miller S. (1999) Folding of coliphage T4 short tail fiber in vitro. Analysing the role of a bacteriophage-encoded chaperone. Eur. J. Biochem. **265:** 771–778
61 King J. and Mykolajewycz N. (1973) Bacteriophage T4 tail assembly: proteins of the sheath, core, and baseplate. J. Mol. Biol. **75:** 339–358
62 Moody M. F. and Makowski L. (1981) X-ray diffraction study of tail-tubes from bacteriophage T2L. J. Mol. Biol. **150:** 217–244
63 Lepault J. and Leonard K. (1985) Three-dimensional structure of unstained frozen-hydrated extended tails of bacteriophage T4. J. Mol. Biol. **182:** 431–441

64 Caspar D. L. D. (1980) Movement and self-control in protein assemblies: quasi-equivalence revisited. Biophys. J. **32:** 103– 138
65 Arisaka F., Engel J. and Klump H. (1981) Contraction and dissociation of the bacteriophage T4 tail sheath induced by heat and urea. In: Bacteriophage Assembly, pp. 365–379, DuBow M. (ed.), Liss, New York
66 Amos L. A. and Klug A. (1975) Three-dimensional image reconstruction of the contractile tail of T4 bacteriophage. J. Mol. Biol. **99:** 51–64
67 Kikuchi Y. and King J. (1975) Genetic control of bacteriophage T4 baseplate morphogenesis. I. Sequential assembly of the major precursor, in vivo and in vitro. J. Mol. Biol. **99:** 645–672
68 Kikuchi Y. and King J. (1975) Genetic control of bacteriophage T4 baseplate morphogenesis. II. Mutants unable to form the central part of the baseplate. J. Mol. Biol. **99:** 673–694
69 Kikuchi Y. and King J. (1975) Genetic control of bacteriophage T4 baseplate morphogenesis. III. Formation of the central plug and overall assembly pathway. J. Mol. Biol. **99:** 695–716
70 Kozloff L. M. (1981) Composition of the T4D bacteriophage baseplate and the binding of the central tail plug. In: Bacteriophage Assembly, pp. 327–342, DuBow M. (ed.), Liss, New York
71 Plishker M. F., Chidambaram M. and Berget P. B. (1983) Isolation and characterization of precursors in bacteriophage T4 baseplate assembly. II. Purification of the protein products of genes *10* and *11* and the in vitro formation of the P(10/11) complex. J. Mol. Biol. **170:** 119–135
72 Watts N. R. M. and Coombs D. H. (1990) Structure of the bacteriophage T4 baseplate as determined by chemical cross-linking. J. Virol. **64:** 143–154
73 Watts N. R. M., Hainfeld J. and Coombs D. H. (1990) Localization of the proteins gp7, gp8 and gp10 in the bacteriophage T4 baseplate with colloidal gold:$F(ab)_2$ and undecagold:Fab′ conjugates. J. Mol. Biol. **216:** 315–325
74 Ferguson P. L. and Coombs D. H. (2000) Pulse-chase analysis of the in vivo assembly of the bacteriophage T4 tail. J. Mol. Biol. **297:** 99–117
75 Zhao L., Takeda S., Inoue M., Leiman P. G. and Arisaka F. (2000) Stoichiometry and inter-subunit interaction of the wedge initiation complex, gp10-gp11, of bacteriophage T4. Biochim. Biophys. Acta **1479:** 286–292
76 Kostyuchenko V. A., Navruzbekov G. A., Kurochkina L. P., Strelkov S. V., Mesyanzhinov V. V. and Rossmann M. G. (1999) The structure of bacteriophage T4 gene product 9: the trigger for tail contraction. Structure **7:** 1213–1222
77 Raaij M. J. van, Schoehn G., Burda M. R. and Miller S. (2001) Crystal structure of a heat and protease-stable part of the bacteriophage T4 short tail fibre. J. Mol. Biol. **314:** 1137–1146
78 Leiman P. G., Kostyuchenko V. A., Shneider M. M., Kurochkina L. P., Mesyanzhinov V. V. and Rossmann M. G. (2000) Structure of bacteriophage T4 gene product 11, the interface between the baseplate and short tail fibers. J. Mol. Biol. **301:** 975–985
79 Shneider M. M., Boudko S. P., Lustig A. and Mesyanzhinov V. V. (2001) Properties of bacteriophage T4 baseplate protein encoded by gene 8. Biochemistry (Moscow) **66:** 693–697
80 Kanamaru S., Leiman P. G., Kostyuchenko V. A., Chipman P. R., Mesyanzhinov V. V., Arisaka F. et al. (2002) The structure of the bacteriophage T4 cell-puncturing device. Nature **415:** 553–557
81 Abuladze N. K., Gingery M., Tsai J. and Eiserling F. A. (1994) Tail length determination in bacteriophage T4. Virology **199:** 301–310
82 Nieradko J. and Koszalka P. (1999) Evidence of interactions between Gp27 and Gp28 constituents of the central part of bacteriophage T4 baseplate. Acta Microbiol. Pol. **48:** 233–242
83 Ishimoto L. K., Ishimoto K. S., Cascino A., Cipollaro M. and Eiserling F. A. (1988) The structure of three bacteriophage T4 genes required for tail-tube assembly. Virology **164:** 81–90
84 King J. (1968) Assembly of the tail of bacteriophage T4. J. Mol. Biol. **32:** 231–262
85 Vianelli A., Wang G. R., Gingery M., Duda R. L., Eiserling F. A. and Goldberg E. B. (2000) Bacteriophage T4 self-assembly: localization of gp3 and its role in determining tail length. J. Bacteriol. **182:** 680–688
86 Arisaka F., Nakako T., Takahashi H. and Ishii S. (1988) Nucleotide sequence of the tail sheath gene of bacteriophage T4 and amino acid sequence of its product. J. Virol. **62:** 1186–1193
87 Zhao L., Kanamaru S., Chaidirek C. and Arisaka F. (2003) P15 and P3, the tail completion proteins of bacteriophage T4, both form hexameric rings. J. Bacteriol. **185:** 1693–1700
88 Mosig G., Lin G. W., Franklin J. and Fan W. H. (1989) Functional relationships and structural determinants of two bacteriophage T4 lysozymes: a soluble (gene e) and a baseplate-associated (gene 5) protein. New Biol. **1:** 171–179
89 Matthews B. W. and Remington S. J. (1974) The three dimensional structure of the lysozyme from bacteriophage T4. Proc. Natl. Acad. Sci. USA **71:** 4178–4182
90 Kanamaru S., Gassner N. C., Ye N., Takeda S. and Arisaka F. (1999) The C-terminal fragment of the precursor tail lysozyme of bacteriophage T4 stays as a structural component of the baseplate after cleavage. J. Bacteriol. **181:** 2739–2744
91 Makhov A. M., Trus B. L., Conway J. F., Simon M. N., Zurabishvili T. G., Mesyanzhinov V. V. et al. (1993) The short tail-fiber of bacteriophage T4: molecular structure and a mechanism for its conformational transition. Virology **194:** 117–127
92 Nakagawa H., Arisaka F. and Ishii, S. (1985) Isolation and characterization of the bacteriophage T4 tail-associated lysozyme. J. Virol. **54:** 460–466
93 Riede I. (1987) Receptor specificity of the short tail fibres (gp12) of T-even type *Escherichia coli* phages. Mol. Gen. Genet. **206:** 110–115
94 Tao Y., Strelkov S.V., Mesyanzhinov V.V. and Rossmann M.G. (1997) Structure of bacteriophage T4 fibritin: a segmented coiled coil and the role of the C-terminal domain. Structure **5:** 789–798
95 Onorato L., Stirmer B. and Showe M. K. (1978) Isolation and characterization of bacteriophage T4 mutant preheads. J. Virol. **27:** 409–426
96 Isobe E., Black L. W. and Tsugita A. (1976) Protein cleavage during virus assembly: a novel specificity of assembly dependent cleavage in bacteriophage T4. Proc. Natl. Acad. Sci. USA **73:** 4205–4209
97 Simpson A. A., Leiman P. G., Tao Y., He Y., Badasso M. O., Jardine P. J. et al. (2001) Structure determination of the head-tail connector of bacteriophage ϕ29. Acta Crystallogr. **D57:** 1260–1269
98 Sandmeier H., Iida S. and Arber W. (1992) DNA inversion regions Min of plasmid p15B and Cin of bacteriophage P1: evolution of bacteriophage tail fiber genes. J. Bacteriol. **174:** 3936–3944
99 Lawrence C. E., Altschul S. F., Boguski M. S., Liu J. S., Neuwald A. F. and Wootton J. C. (1993) Detecting subtle sequence signals: a Gibbs sampling strategy for multiple alignment. Science **262:** 208–214